scientific reports

Check for updates

OPEN

Exploring the potential of standalone and tandem solar cells with Sb_2S_3 and Sb_2Se_3 absorbers: a simulation study

Z. Dahmardeh & M. Saadat✉

Thin-film antimony chalcogenide binary compounds are potential candidates for efficient and low-cost photovoltaic absorbers. This study investigates the performance of Sb_2S_3 and Sb_2Se_3 as photovoltaic absorbers, aiming to optimize their efficiency. The standalone Sb_2S_3 and Sb_2Se_3 sub-cells are analyzed using SCAPS-1D simulations, and then a tandem structure with Sb_2S_3 as the top-cell absorber and Sb_2Se_3 as the bottom-cell absorber is designed, using the filtered spectrum and the current matching technique. The optimal configuration for maximum efficiency is achieved by adjusting the thickness of the absorber layer. The results show that antimony chalcogenide binary compounds have great potential as photovoltaic absorbers, enabling the development of efficient and low-cost solar cells. A remarkable conversion efficiency of 22.2% is achieved for the optimized tandem cell structure, with absorber thicknesses of 420 nm and 1020 nm for the top and bottom sub-cells respectively. This study presents a promising approach towards high-performance tandem solar cells.

Research is being conducted into alternative energy sources in order to identify options that are both cost-effective and environmentally friendly. As part of this research, bulk and thin film materials are being investigated as potential photovoltaic absorbers[1–5]. There has been increasing interest in the photovoltaic applications of antimony chalcogenide binary compounds, including Sb_2S_3, Sb_2Se_3, and mixed antimony chalcogenide $Sb_2(S,Se)_3$[6–10]. As well as having a high optical absorption coefficient ($>10^5$ cm^{-1} in the visible range), antimony chalcogenide binary compounds have a long carrier lifetime, adjustable band gaps (1.2 eV for Sb_2Se_3 and 1.7 eV for Sb_2S_3), decent carrier mobility, earth-abundant, long-term stability, low toxicity, moisture, and air stability[6,11–17]. Also, antimony chalcogenide thin films have been effectively prepared using both vacuum and non-vacuum processes[18–21]. Maximum efficiency of more than 10% has been achieved with antimony chalcogenide-based solar cells[22]. These characteristics make antimony chalcogenide compounds promising alternatives to existing thin-film photovoltaic technologies.

A typical single-junction solar cell uses only a portion of the solar spectrum; the rest is reflected or lost as heat (Shockley-Queisser limit). By using tandem solar cells, the Shockley-Queisser limit of single-junction solar cells can be exceeded, resulting in increased power generation under certain light conditions[8]. Tandem solar cells consist of a top cell with a high band gap that absorbs short wavelength solar radiation and a bottom cell with a low band gap that absorbs longer wavelength solar radiation. An open circuit voltage (V_{OC}) for a tandem device is predicted to be the sum of the V_{OC}s for each of its sub-cells. It is important to note, however, that the current density of a serial tandem cell is limited to that of the lower current density of the sub-cell, resulting in a large current loss when the current densities of the sub-cells are mismatched[23,24]. A major objective of this project is to develop the most efficient solar cell possible, which will consist of several layers with different band gaps. Having a band gap of 1.2 eV, Sb_2Se_3 is an excellent candidate for the bottom cell material in tandem solar cells, while Sb_2S_3, with a band gap of 1.7 eV, is an excellent candidate for the top cell material[8,25,26].

Sb_2S_3 has been suggested as a possible top sub-cell candidate for coupling with c-Si, CIGSe, CdTe, $Cu_2ZnSnSe_4$, and $Cu_2ZnSn(S, Se)_4$ as bottom sub-cell candidates[8,27]. For example in a study conducted by Okil et al., the researchers focused on Sb_2S_3/Si tandem solar cells. They performed optimizations on various parameters to improve the cell's performance. As a result of these optimizations, they achieved an impressive efficiency of 23.25%[28]. Alanazi et al., conducted a simulation study introducing a 2T Organic/Sb_2Se_3 tandem device. The study explored inverted (p-i-n)/(p-i-n) and conventional (n-i-p)/(n-i-p) configurations. Through optimization and current matching, the inverted tandem cell achieved an impressive power conversion efficiency (PCE) of

Department of Physics, University of Sistan and Baluchestan, Zahedan, Iran. ✉email: Saadat@phys.usb.ac.ir

21.52%, while the conventional tandem cell achieved a PCE of 19.14%. The initial standalone top and bottom cells exhibited efficiencies of 9.45% and 7.89% respectively[29]. The crystal structures and characteristics of Sb_2S_3 and Sb_2Se_3 are, however, similar. By utilizing these materials, tandem cells may be able to be made that are stable, cost-effective, and environmentally friendly[8,25,30]. In 2020, Zhang et al., developed a tandem solar cell utilizing antimony chalcogenide compounds. By employing Sb_2S_3 and Sb_2Se_3 as the top and bottom cells, respectively, they achieved an efficiency of 7.93%, surpassing the efficiencies of the individual top and bottom single solar cells. This study highlights the potential of antimony chalcogenides for tandem solar cell applications[31]. Cao's study revealed a remarkable efficiency of 26.64% for Sb_2S_3/Sb_2Se_3 tandem solar cells after removing the defect state in the light-absorbing layer[25]. The recent simulation of tandem solar cells with the structure $Mo/Sb_2Se_3/Sb_2S_3/CdS/i\text{-}ZnO/ZnO:Al$ was carried out by Bal et al. A tandem cell with 13.2% efficiency was achieved after optimization of the different parameters[32]. Dahmardeh et al., investigated how the performance of $Sb_2(S,Se)_3/Sb_2(S,Se)_3$ tandem solar cells changed with different amounts of selenium in the absorber layers. They found that the energy gap between the two sub-cells influenced the current flow. They obtained the best conversion efficiency of 22.19% by adjusting the Se/(Se + Se) ratio in the absorber layers[33].

In this study, we created and analyzed single Sb_2S_3 and Sb_2Se_3 solar cells, as well as tandem Sb_2S_3/Sb_2Se_3 devices using the Solar Cell Capacitance Simulator (SCAPS) software[34]. We will first discuss the modeling and simulation results for the singular Sb_2S_3 and Sb_2Se_3 solar cell structures. In the next step, we will report the results of our simulation of tandem Sb_2S_3/Sb_2Se_3 solar cells. During this configuration, Sb_2S_3 acts as the absorber layer at the top of the cell and Sb_2Se_3 acts as the absorber layer at the bottom of the cell. Since mismatched current density is the primary source of current loss in tandem cells, it was decided to adjust the absorber thickness of the sub-cells in order to determine the "current matching" point where the sub-cells possess equal short circuit current densities. In comparison with the individual Sb_2S_3 and Sb_2Se_3 devices, the tandem cell combining these two materials demonstrated enhanced photovoltaic efficiency.

Methodology

An example of a single junction solar cell is shown in Fig. 1. As the absorber layer, this device contains Sb_2S_3 or Sb_2Se_3, CdS as the electron transport layer (ETL), and SpiroOMeTAD as the hole transport layer (HTL), as well as Au and FTO acting as back and front contacts, respectively. Simulations of single junction devices were conducted using the SCAPS software. The program is based on numerical solutions of the Poisson equation, current density equations for electrons and holes, and continuity equations for holes and electrons with appropriate boundary conditions at interfaces and contacts[13,35].

In the first step, a model based on experimental data[22] was used to design independent single junction sub-cells comprised of SnO_2:F/ETL (CdS)/absorber/HTL (SpiroOMeTAD)/Au. Based on the previous research work reported in the literature, we have selected the material parameters and presented them in Table 1S[13,33,36]. We have used different dielectric permittivity and electron and hole mobility for the Sb_2S_3/Sb_2Se_3 absorber layer[25]. A neutral defect with a density of 1.4×10^{12} cm^{-2} was assumed at both the ETL/absorber and HTL/absorber interfaces. We have also taken into account the bulk defects reported for record $Sb_2(S, Se)_3$ solar cells in the absorber layers[22]. In addition, we have assumed an internal defect near the midgap states for HTL, ETL, and FTO layers. The defect state parameters for the absorber, HTL, ETL, and FTO layers are shown in Table 2S. We have obtained all the other input parameters for the simulation of solar cells from the literature[36] or logically assumed them to prevent misleading or unrealistic results. The spectral conditions for all simulations are 1.5 AM and the operating temperature is 300 K. Table 3S shows a comparison of the experimental and simulated solar cells data. The good consistency between the simulated results and the experimental data confirms the validity of our model.

There are two types of absorber layers in the top and bottom sub-cells, with Sb_2S_3 on the top and Sb_2Se_3 on the bottom. A relationship was established between the performance of the sub-cells and the thickness of the absorber layer. We used the AM 1.5 G spectrum and a temperature of 300 K for standalone simulations of top and bottom sub-cells.

An absorber layer's band gap determines the number of photons that can be absorbed by a single junction solar cell. It is possible to enhance the performance of photovoltaic systems by using tandem structures. In tandem cells containing Sb_2S_3/Sb_2Se_3, the top cell contains an absorber layer with a band gap of 1.7 eV and the

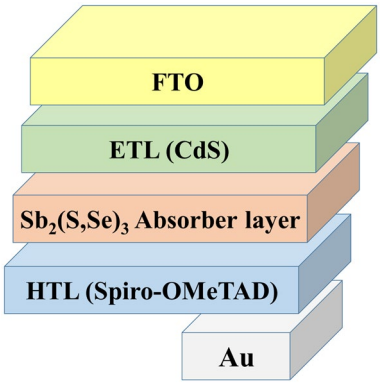

Figure 1. Device architecture of $Sb_2(S,Se)_3$ solar cell used in the numerical simulation.

bottom cell contains an absorber layer with a band gap of 1.2 eV. After evaluating the performance of Sb_2S_3-based top and Sb_2Se_3-based bottom cells, the Sb_2S_3/Sb_2Se_3 tandem structure was analyzed.

We can simulate a tandem architecture in SCAPS by connecting the top and bottom cells using the current matching technique[23]. The Sb_2S_3 top cell is illuminated by the standard global AM 1.5 G spectrum; however, the Sb_2Se_3 bottom cell is illuminated by the residual solar spectrum after partial absorption across the top cell. Using this equation[24], we can calculate the spectrum passing through the top sub-cell with varying Sb_2S_3 thicknesses to the bottom sub-cell:

$$T(\lambda) = T_0(\lambda)\exp\left[\sum_{k=1}^{n} -(\alpha_k(\lambda)t_k)\right] \quad (1)$$

This is the incident standard global AM 1.5 G spectrum, the layer number, represents the number of layers of the top sub-cell, and the thickness of each layer represents T0(λ), k, n and t respectively. Also, α(λ) is the absorption coefficient of each material and given by[24]:

$$\alpha(E) = A_\alpha\sqrt{h\nu - E_g} \quad (2)$$

where Aα, Eg, h, and ν are pre-factor, the energy gap of the material (eV), the Planck's constant (eV.sec), and the spectrum frequency respectively. The Fig. 2 illustrates the schematic of a Sb_2S_3/Sb_2Se_3 tandem device with

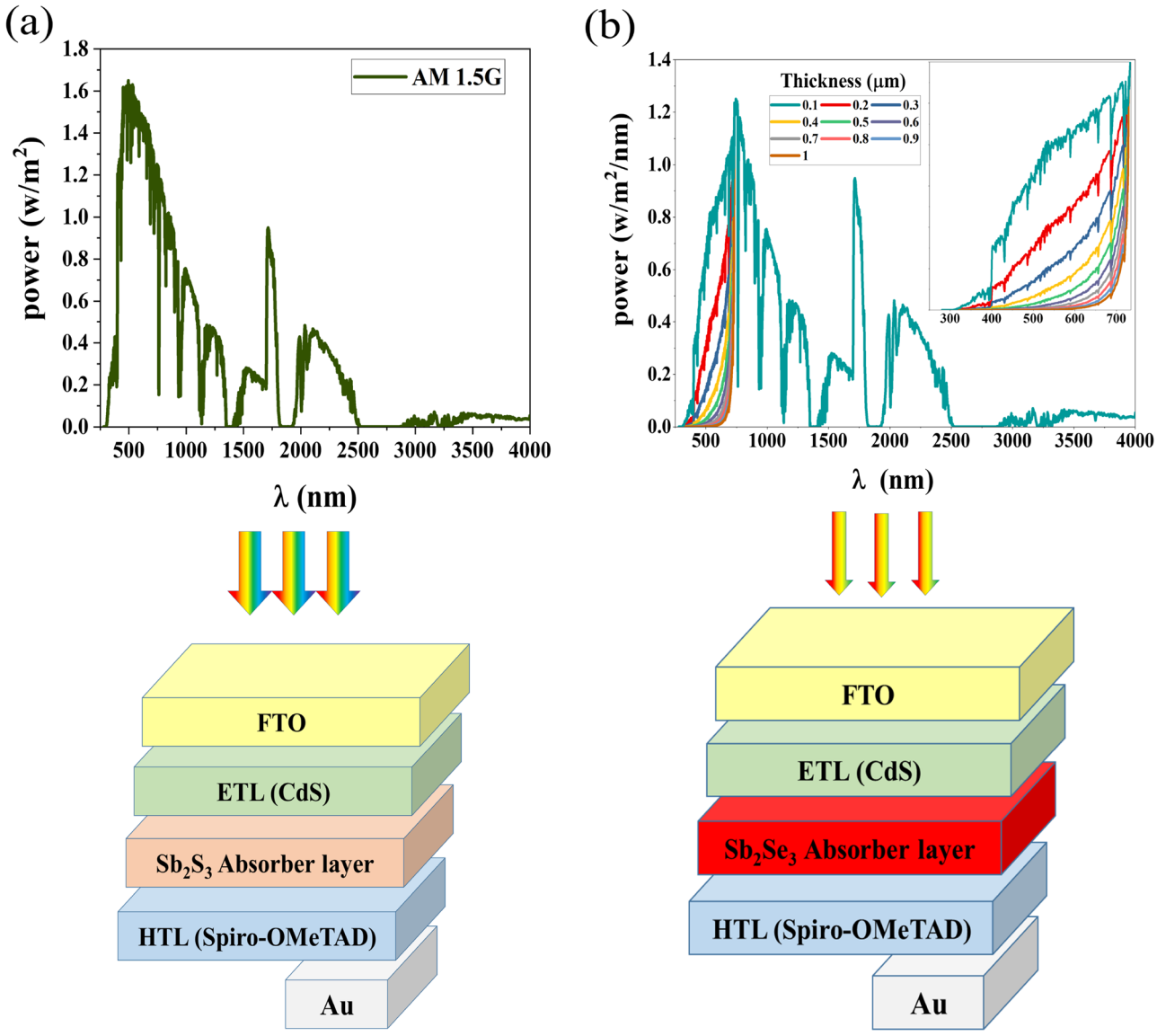

Figure 2. Schematic diagram of tandem cell with (**a**) AM1.5 spectrum at the top sub-cell and (**b**) filtered spectrum transmitted by top sub-cell with different absorber layer thickness at bottom sub-cell.

an incident AM 1.5 G spectrum to the Sb_2S_3 top sub-cell and a filtered spectrum to the Sb_2Se_3 bottom sub-cell. Each sub-cell has an absorber layer that absorbs photons with an energy greater than the band gap. The thickness of top and bottom sub-cells was altered in order to achieve equal current density across both. The monolithic tandem solar cell must meet this requirement.

Results and discussions

Simulation of Sb_2S_3 top cell

This section focuses on simulating the Sb_2S_3 top sub-cell. Simulations of top sub-cells were conducted using the standard AM 1.5 G spectrum. A study was conducted to examine the effect of the thickness of the absorber layer on the Sb_2S_3 sub-cell. The thickness of the absorber layer was varied between 50 nm and 2 µm. Figures 3 and 4 present the J–V characteristics, external quantum efficiency (EQE), and photovoltaic parameters, respectively, of Sb_2S_3 solar cells with varying absorber layer thicknesses. By increasing the absorbance layer thickness to 650 nm, J_{SC} increased to 21.2 mA cm^{-2} as a result of increased absorption and generation rates. Further increases in thickness beyond 650 nm, however, resulted in saturation of absorption and little change in J_{SC} values. There is an increase in recombination in the thicker Sb_2S_3 absorber as a result of the addition of a 1.25 µm thick Sb_2S_3 layer[23]. According to external quantum efficiency spectra, photon harvesting was improved up to 1–1.2 µm, after which it began to decline for wavelengths less than 730 nm. As a result of this decrease in response, J_{SC} values decreased. As the thickness of the Sb_2S_3 absorber increased from 50 nm to 2 µm, V_{OC} reduced slightly from 590 to 545 mV and fill factor (FF) from 70.42 to 28.47%. The reduced electric field across the thick Sb_2S_3 layer is the cause of the decreased V_{OC} and FF in the device (Fig. 5). The lower electric field reduces the probability of charge carrier separation, thus reducing the V_{OC} and FF[23,37]. An increase in J_{SC} increases power conversion efficiency (PCE) for thicknesses less than 350 nm. In contrast, when it comes to thicker films, it is the reduction of V_{OC}s and FF that becomes the determining factor. Accordingly, PCE was initially increased, followed by a decrease as thickness increased, with a maximum PCE value of 6.65% at 350 nm thick Sb_2S_3.

Simulation of Sb_2Se_3 bottom cell

In this section, the study of simulating the Sb_2Se_3 bottom sub-cell is performed. For standalone simulations of bottom sub-cell, the standard AM 1.5 G spectrum was employed. J–V characteristics of the Sb_2Se_3 bottom

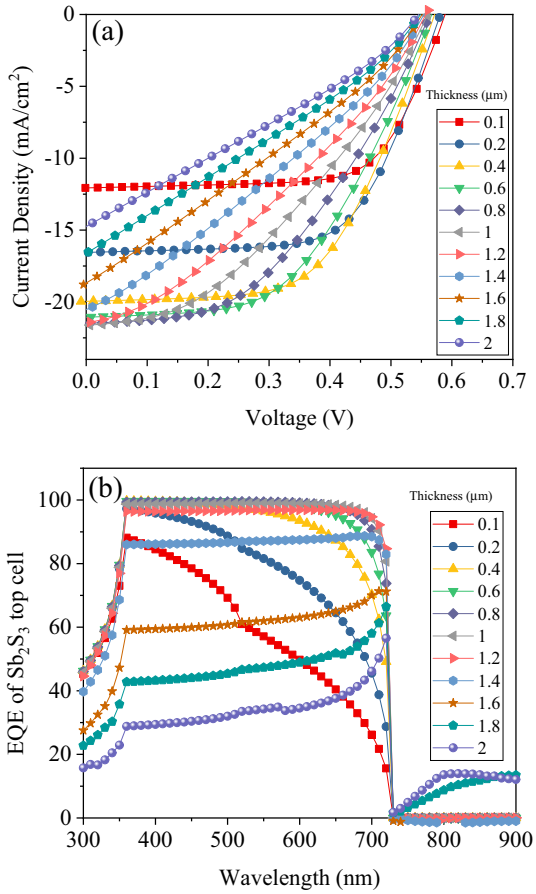

Figure 3. (**a**) J–V curve and (**b**) EQE of Sb_2S_3 based top cell with absorber thickness in a standalone configuration.

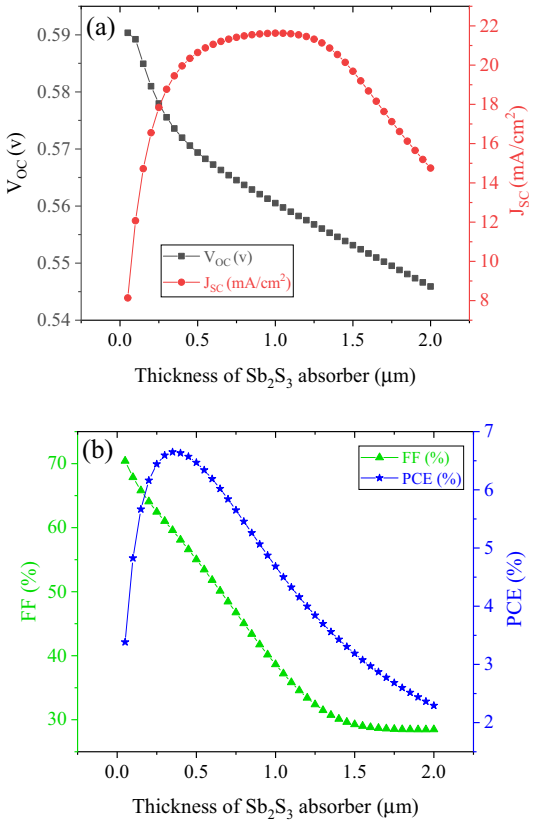

Figure 4. Photovoltaic characteristics of Sb_2S_3 based top cell with absorber thickness: (**a**) V_{OC} and J_{SC} and (**b**): FF and PCE.

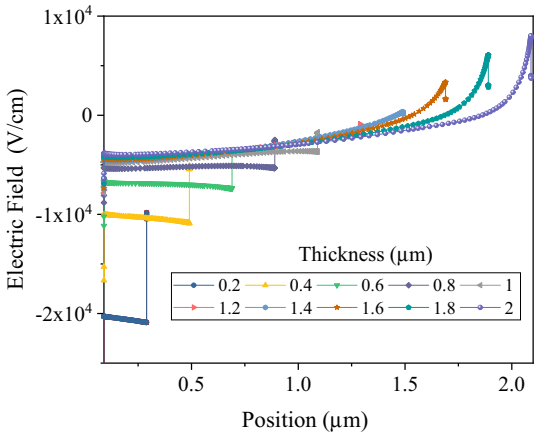

Figure 5. Electric field strength across the top cell Sb_2S_3 absorber layer with absorber thickness.

sub-cell for different values of absorbing layer thickness are shown in Fig. 6a. Extracted from the different J–V characteristics in Fig. 6, the photovoltaic parameters of Sb_2S_3 solar cells with different absorber thickness is illustrated in Fig. 7. We discovered that Sb_2Se_3 solar cells have a relatively lower open circuit voltage than Sb_2S_3 absorber layer-based solar cells, as shown in Fig. 7a, because Sb_2Se_3 has a smaller band gap than Sb_2S_3 absorber layer[38,39]. A slight increase in the V_{OC} of Sb_2Se_3 solar cells is observed as thickness of absorber grows, reaching its maximum value. This is mostly due to the fact that a thicker Sb_2Se_3 absorber layer will absorb more photons, contributing to the production of electron–hole pairs[40]. Figure 7a shows that increasing the absorbance layer thickness up to 700 nm resulted in an increase in J_{SC} to 38.0 mA cm^{-2} due to enhanced absorption and generation rates. However, further increases in thickness beyond 700 nm led to saturation of absorption and little change in J_{SC} values. The external quantum efficiency spectra of Sb_2S_3 sub-ells with various thicknesses are depicted in Fig. 6b. The absorber layer's photon harvesting improved with an increase in thickness of up to 0.8 µm. However,

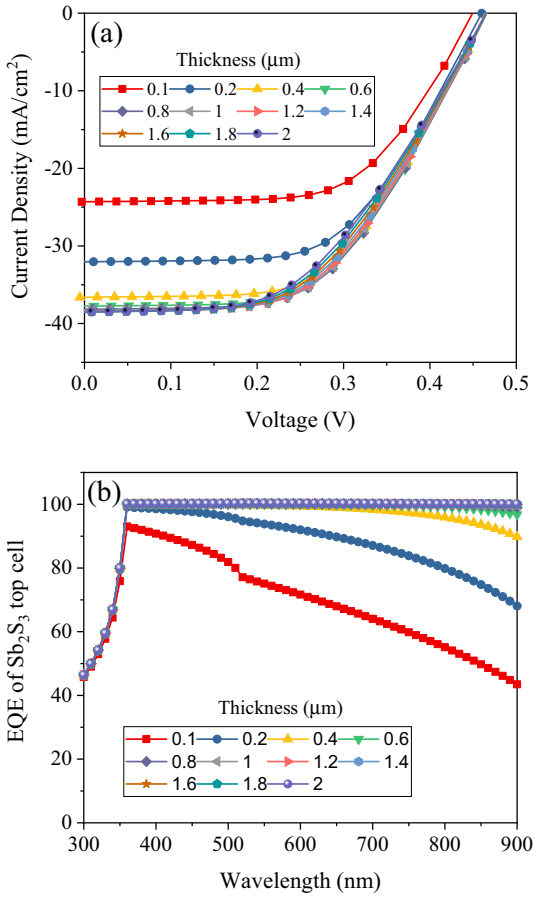

Figure 6. (**a**) J–V curve and (**b**) EQE of Sb_2Se_3 based bottom cell with absorber thickness in a standalone configuration.

as thickness rises above this point, the optical absorption virtually reaches saturation. This also verifies the variation in the J_{SC} as mentioned earlier. In Fig. 7b, it is visible that the FF is greatly dropped from 63.4% for 50 nm to 48.9% for 2.0 μm. As the thickness of these single junction solar cells increases, so does their efficiency, peaking at 0.5–0.7 μm. After that, efficiency starts to drop off as thickness continues to increase.

Simulation of Sb_2S_3/Sb_2Se_3 tandem solar cell

In this part, the performance of Sb_2S_3/Sb_2Se_3 tandem solar cells is explored utilizing a filtered spectrum (described in the "Methodology" section) combined with a current matching process. The filtered spectrum and integrated power are shown in Fig. 8 for different thicknesses of the absorber layer in the top cell. The filtered spectrum clearly illustrates that with increasing Sb_2S_3 thickness, power passed to the bottom cell decreases, especially at wavelengths below 730 nm. Furthermore, Fig. 8b shows that the integrated power transmitted by the top cell decreases as the thickness of the absorber layer decreases.

Having equal currents in both sub-cells is crucial for monolithic tandem solar cells[23,24]. Thus, both the upper and lower sub-cell thicknesses must be adjusted at the same time in order to achieve current matching. For each sub-cell, the thickness of the top cell was altered in 100 nm steps while the thickness of the bottom cell was changed until an identical J_{SC} was obtained. In the top cell, AM 15 G spectrum is used to illuminate the cell, and in the bottom cell, a filtered spectrum is used to illuminate the cell. Therefore, the J_{SC} for the lower sub-cell is altered as a result of the thickness of the absorb layer in both cells, while for the upper cell the J_{SC} is altered as a result of the thickness of the absorb layer in only one cell.

J-V curves are presented in Fig. 9 for different thicknesses of Sb_2S_3/Sb_2Se_3 tandem solar cells. At different current matching points, Fig. 10 illustrates the fluctuation of photovoltaic characteristics of tandem solar cells. Compared to the single device, the tandem device exhibits improved values of J_{SC} at higher current matching points. With a 430 nm (top absorber)/1310 nm (bottom absorber) configuration, the highest J_{SC} value was achieved. Current matching requires thicker bottom absorbers for thicker top absorbers; for example, 450 nm thick top absorbers require 6 μm thick bottom absorbers. In order to minimize material consumption, keeping the top layer within 400–430 nm is more efficient. A comparison of V_{OC} of tandem solar cells for different current matching points shows that V_{OC} to FF ratios decrease at higher current matching points. As shown in Fig. 10b, the PCE of the tandem cell under matching conditions can be determined. As cell thickness increases,

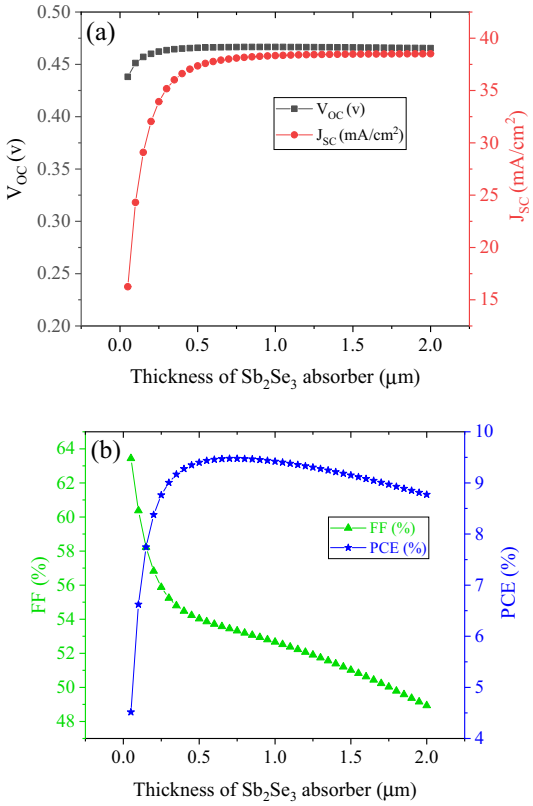

Figure 7. Photovoltaic characteristics of Sb_2Se_3 based bottom cell with absorber thickness: (**a**) V_{OC} and J_{SC} and (**b**): FF and PCE.

efficiency increases until it reaches a plateau at or beyond 400 nm for the upper sub-cell. 420 nm and 1020 nm are the optimal thicknesses for the top and bottom sub-cells of a tandem device (Fig. 10b). The efficiency of the system becomes saturated when the value is exceeded. Figure 2 illustrates the structure of this device, illuminated by AM 1.5 G incident spectrum on the top sub-cell of Sb_2S_3 and filtered AM 1.5 G on the bottom sub-cell of Sb_2Se_3. Figure 11 shows the J–V curve of each sub-cell along with their combined tandem solar cell counterpart.

Figure 12 illustrates the spectrum of Sb_2S_3, Sb_2Se_3, and the Sb_2S_3/Sb_2Se_3 tandem device. Additionally, Fig. 13 illustrates the external quantum efficiency of both sub-cells. As illustrated by the quantum efficiency curve in Fig. 13, photon energy was more effectively taken in at longer wavelengths from the bottom cell with a lower band gap and shorter wavelengths from the top cell with a higher band gap, resulting in the generation of current at a wide range of frequencies. At wavelengths up to 729 nm ($h\nu > 1.7$ eV), the upper cell is shown to be dominant in the EQE versus wavelength plots. For longer wavelengths ($h\nu < 1.7$ eV) however, the upper cell becomes virtually invisible and absorption from the bottom cell increases, resulting in improved quantum efficiency across a broad range.

Conclusions

Photovoltaic systems can be improved by using tandem structures. The performance of the Sb_2S_3 and Sb_2Se_3 sub-cells when operating independently was examined, after which the tandem structure of Sb_2S_3/Sb_2Se_3 was explored. The tandem structure had a power conversion efficiency that was much higher than the standalone cells. In order to achieve "current matching"—a point at which thesub-cells have the same J_{SC}—and reduce current loss due to amismatch of current density, it was necessary to change the thickness of the absorber in tandem cells. For thicker top absorbers, higher thicknesses of bottom absorbers are required for current matching. To minimize material usage we propose that the thickness of top layer choose within 400–430 nm range. This Sb_2S_3/Sb_2Se_3 tandem solar cell yielded an impressive conversion efficiency of 22.2%, with 420 nm and 1020 nm thick absorber layers for its top and bottom sub-cells respectively. The other photovoltaic parameters are J_{SC} (20.15 mA cm^{-2}), V_{OC} (1.02 V), and FF (59.58%). This research on the Sb_2S_3/Sb_2Se_3 tandem design can lead to the production of high-performance tandem solar cells.

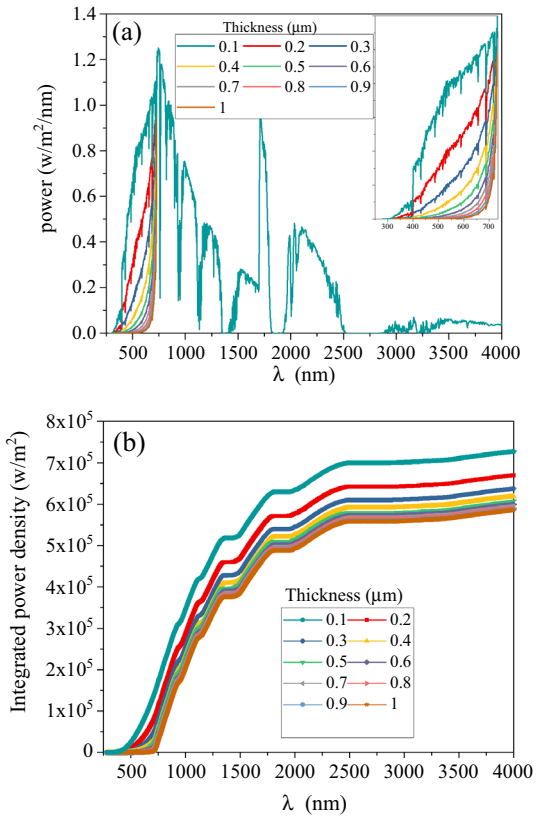

Figure 8. (**a**) Filtered spectrum and (**b**) integrated power density transmitted by top cell with different absorber layer thickness.

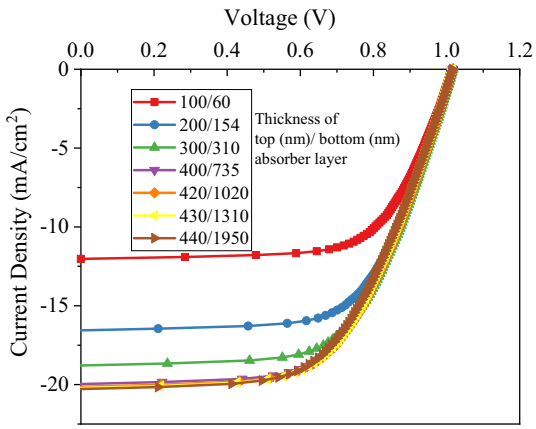

Figure 9. J–V curve of Sb_2S_3/Sb_2Se_3 tandem with thicknesses corresponding to first seven current matching points.

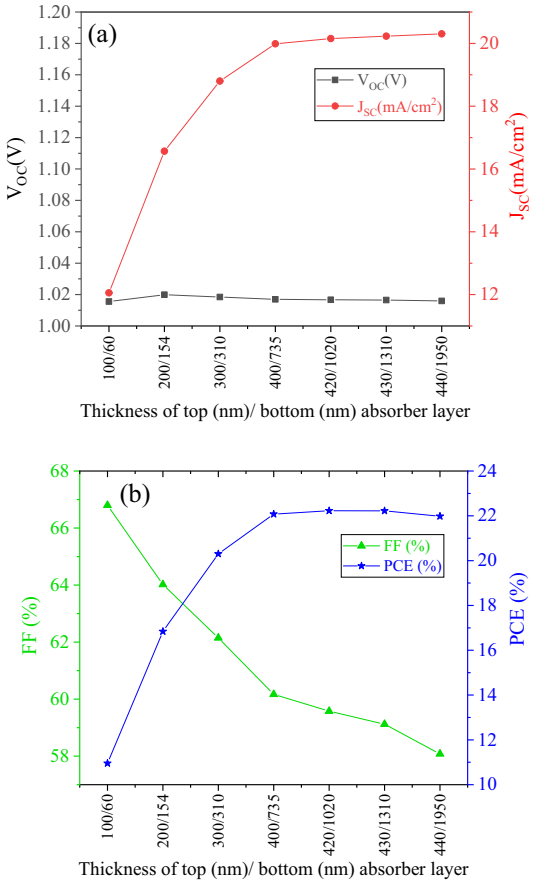

Figure 10. Photovoltaic characteristics of Sb_2S_3/Sb_2Se_3 tandem solar cell with thicknesses corresponding to the first seven current matching points: (**a**) V_{OC} and J_{SC} and (**b**): FF and PCE.

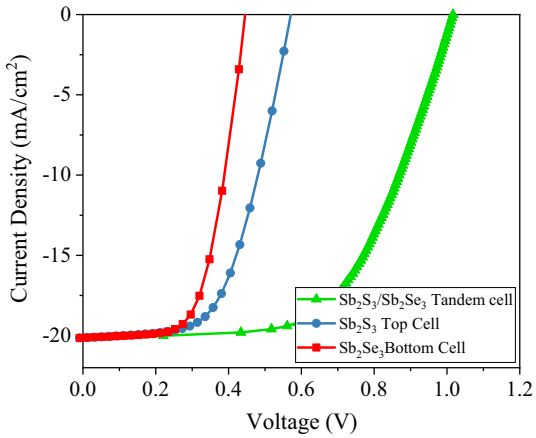

Figure 11. Illuminated J–V curves of standalone Sb_2S_3 top and Sb_2Se_3 bottom sub-cells at optimized thickness (420 nm/1020 nm), bottom cell under filtered spectrum by top cell, and Sb_2S_3/Sb_2Se_3 tandem solar cell.

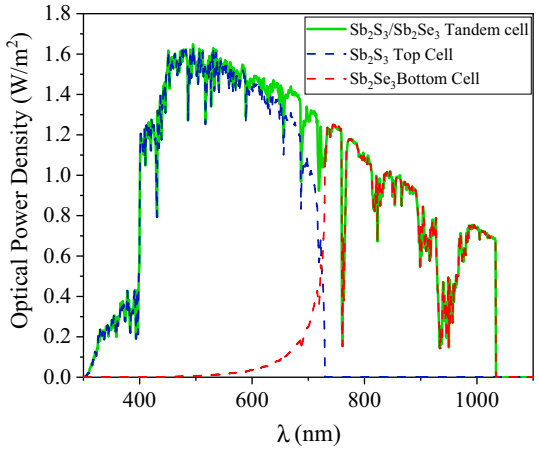

Figure 12. The absorbed spectrum of Sb_2S_3, Sb_2Se_3 sub-cells, and Sb_2S_3/Sb_2Se_3 tandem cell.

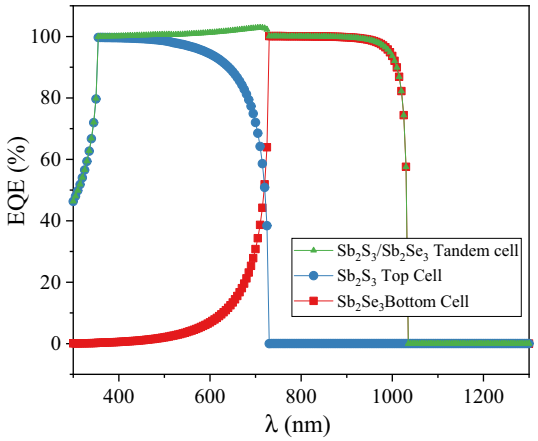

Figure 13. EQE of Sb_2S_3 and Sb_2Se_3 sub-cells.

Data availability

The data that support the findings of this study are available from the corresponding author upon reasonable request.

Received: 28 September 2023; Accepted: 6 December 2023
Published online: 19 December 2023

References

1. Wang, Y. *et al.* Research progress in doped absorber layer of CdTe solar cells. *Renew. Sustain. Energy Rev.* **2023**, 113427 (2023).
2. Choudhury, B. D. *et al.* The photon absorber and interconnecting layers in multijunction organic solar cell. *Sol. Energy* **201**, 28–44 (2020).
3. Lingg, M., Buecheler, S. & Tiwari, A. N. Review of CdTe1− x Se x thin films in solar cell applications. *Coatings* **9**, 520 (2019).
4. Suresh, S. & Uhl, A. R. Present status of solution-processing routes for Cu (In, Ga)(S, Se) 2 solar cell absorbers. *Adv. Energy Mater.* **11**, 2003743 (2021).
5. Sharma, R., Sharma, A., Agarwal, S. & Dhaka, M. Stability and efficiency issues, solutions and advancements in perovskite solar cells: A review. *Sol. Energy* **244**, 516 (2022).
6. Mavlonov, A. *et al.* A review of Sb2Se3 photovoltaic absorber materials and thin-film solar cells. *Sol. Energy* **201**, 227–246 (2020).
7. Chen, C., Li, K. & Tang, J. T. years of Sb2Se3 thin film solar cells. *Solar RRL* **6**, 2200094 (2022).
8. Shah, U. A., Chen, S., Khalaf, G. M. G., Jin, Z. & Song, H. Wide bandgap Sb2S3 solar cells. *Adv. Funct. Mater.* **31**, 2100265 (2021).
9. Farhana, M. A., Manjceevan, A. & Bandara, J. Recent advances and new research trends in Sb2S3 thin film based solar cells. *J. Sci. Adv. Mater. Dev.* **8**, 100533 (2023).
10. Marín, M. M. N., González-Castillo, J., Vigil-Galán, O. & Piedrahita, M. C. The state of the art of Sb2 (S, Se) 3 thin film solar cells: Current progress and future prospect. *J. Phys. D: Appl. Phys.* (2022).
11. Chen, Z. & Chen, G. The effect of absorber thickness on the planar Sb2S3 thin film solar cell: Trade-off between light absorption and charge separation. *Sol. Energy* **201**, 323–329 (2020).
12. Islam, M. & Thakur, A. Two stage modelling of solar photovoltaic cells based on Sb2S3 absorber with three distinct buffer combinations. *Sol. Energy* **202**, 304–315 (2020).
13. Saadat, M. & Amiri, O. Fine adjusting of charge carriers transport in absorber/HTL interface in Sb2 (S, Se) 3 solar cells. *Sol. Energy* **243**, 163–173 (2022).

14. Choi, Y. C. *et al.* Sb2Se3-sensitized inorganic–organic heterojunction solar cells fabricated using a single-source precursor. *Angew. Chem.* **126**, 1353–1357 (2014).
15. Chen, C. *et al.* Characterization of basic physical properties of Sb2Se3 and its relevance for photovoltaics. *Front. Optoelectron.* **10**, 18–30 (2017).
16. Chen, C. *et al.* Optical properties of amorphous and polycrystalline Sb2Se3 thin films prepared by thermal evaporation. *Appl. Phys. Lett.* **107**, 043905 (2015).
17. Yang, B. *et al.* Hydrazine solution processed Sb2S3, Sb2Se3 and Sb2 (S1− xSex) 3 film: Molecular precursor identification, film fabrication and band gap tuning. *Sci. Rep.* **5**, 10978 (2015).
18. Akshay, V., Benny, S. & Bhat, S. V. Solution-processed antimony chalcogenides based thin film solar cells: A brief overview of recent developments. *Sol. Energy* **241**, 728–737 (2022).
19. Lei, H., Chen, J., Tan, Z. & Fang, G. Review of recent progress in antimony chalcogenide-based solar cells: Materials and devices. *Solar RRL* **3**, 1900026 (2019).
20. Singh, Y., Maurya, K. & Singh, V. A review on properties, applications, and deposition techniques of antimony selenide. *Sol. Energy Mater. Sol. Cells* **230**, 111223 (2021).
21. Wang, J., Li, K., Tang, J. & Chen, C. A perspective of antimony chalcogenide photovoltaics toward commercialization. *Solar RRL* **7**, 2300436 (2023).
22. Tang, R. *et al.* Hydrothermal deposition of antimony selenosulfide thin films enables solar cells with 10% efficiency. *Nat. Energy* **5**, 587–595 (2020).
23. Shrivastav, N., Madan, J., Pandey, R. & Shalan, A. E. Investigations aimed at producing 33% efficient perovskite–silicon tandem solar cells through device simulations. *RSC Adv.* **11**, 37366–37374 (2021).
24. Mousa, M., Amer, F. Z., Mubarak, R. I. & Saeed, A. Simulation of optimized high-current tandem solar-cells with efficiency beyond 41%. *IEEE Access* **9**, 49724–49737 (2021).
25. Cao, Y. *et al.* Rotational design of charge carrier transport layers for optimal antimony trisulfide solar cells and its integration in tandem devices. *Sol. Energy Mater. Sol. Cells* **206**, 110279 (2020).
26. Kondrotas, R., Chen, C. & Tang, J. Sb2S3 solar cells. *Joule* **2**, 857–878 (2018).
27. Lee, T. D. & Ebong, A. U. A review of thin film solar cell technologies and challenges. *Renew. Sustain. Energy Rev.* **70**, 1286–1297 (2017).
28. Okil, M., Shaker, A., Ahmed, I. S., Abdolkader, T. M. & Salem, M. S. Design and analysis of Sb2S3/Si thin film tandem solar cell. *Sol. Energy Mater. Sol. Cells* **253**, 112210 (2023).
29. Alanazi, T. I. *et al.* Proposal and numerical analysis of organic/Sb2Se3 all-thin-film tandem solar cell. *Polymers* **15**, 2578 (2023).
30. Cao, Y. *et al.* Theoretical insight into high-efficiency triple-junction tandem solar cells via the band engineering of antimony chalcogenides. *Solar RRL* **5**, 2000800 (2021).
31. Zhang, J. *et al.* All antimony chalcogenide tandem solar cell. *Solar RRL* **4**, 2000048 (2020).
32. Bal, S. S., Basak, A. & Singh, U. P. Numerical modeling and performance analysis of Sb-based tandem solar cell structure using SCAPS–1D. *Opt. Mater.* **127**, 112282 (2022).
33. Dahmardeh, Z., Saadat, M. & Amiri, O. Enhancing photovoltaic performance of antimony sulfide-selenide tandem solar cells through selenium content variation: Modeling and simulation analysis. *Sol. Energy* **262**, 111788 (2023).
34. Burgelman, M., Nollet, P. & Degrave, S. Modelling polycrystalline semiconductor solar cells. *Thin Solid Films* **361**, 527–532 (2000).
35. Basak, A. & Singh, U. P. Numerical modelling and analysis of earth abundant Sb2S3 and Sb2Se3 based solar cells using SCAPS-1D. *Sol. Energy Mater. Sol. Cells* **230**, 111184 (2021).
36. Nicolás-Marín, M. M., Ayala-Mato, F., Vigil-Galán, O. & Courel, M. Simulation analysis of Cd1-xZnxS/Sb2(Se1-xSx)3 solar cells with n-i-p structure. *Sol. Energy* **224**, 245–252 (2021).
37. Saadat, M., Amiri, O. & Mahmood, P. Analysis and performance assessment of CuSbS2-based thin-film solar cells with different buffer layers. *Eur. Phys. J. Plus* **137**, 1–12 (2022).
38. Gupta, G. K. & Dixit, A. Theoretical studies of single and tandem Cu2ZnSn (S/Se) 4 junction solar cells for enhanced efficiency. *Opt. Mater.* **82**, 11–20 (2018).
39. Saadat, M., Moradi, M. & Zahedifar, M. CIGS absorber layer with double grading Ga profile for highly efficient solar cells. *Superlattices Microstruct.* **92**, 303–307 (2016).
40. Elbar, M., Tobbeche, S. & Merazga, A. Effect of top-cell CGS thickness on the performance of CGS/CIGS tandem solar cell. *Sol. Energy* **122**, 104–112 (2015).

Author contributions

Z.D.: investigation, software. M.S.: conceptualization, investigation, methodology, validation, writing original draft, project administration.

Competing interests

The authors declare no competing interests.

Additional information

Supplementary Information The online version contains supplementary material available at https://doi.org/10.1038/s41598-023-49269-w.

Correspondence and requests for materials should be addressed to M.S.

Reprints and permissions information is available at www.nature.com/reprints.

Publisher's note Springer Nature remains neutral with regard to jurisdictional claims in published maps and institutional affiliations.